# Failure and Stabilization Mechanisms of Graphite Electrodes

**Doron Aurbach,* Mikhail D. Levi, Elena Levi, and Alexander Schechter**

*Department of Chemistry, Bar-Ilan University, Ramat Gan 52900, Israel*

*Received: September 12, 1996; In Final Form: December 12, 1996*[⊗]

The aim of this work was to study failure and stabilization mechanisms of Li−graphite electrodes. As model electrolyte systems, tetrahydrofuran (THF), propylene carbonate (PC), THF containing water contamination, and THF/PC solutions were used. A variety of electrode behavior can be observed in these solutions including reversible intercalation at high capacity, cyclability with deteriorating capacity, and in cases of dry THF and PC solutions, disability of Li intercalation. Chronopotentiometry, chronoamperometry, cyclic voltammetry impedance spectroscopy, electron microscopy, *in situ* and *ex situ* XRD, and surface sensitive FTIR spectroscopy were used in order to understand the reasons for the stability or failure of Li−graphite intercalation anodes. In PC and dry THF, massive solvent reduction occurs with a relatively low degree of electrode passivation. These processes change the electrode's morphology and electrically isolate carbon particles. At low concentration of water (>40 ppm) and PC (optimum 1 M) in THF, the surface chemistry of graphite differs considerably from that in dry THF or PC solutions. Passivating surface films are formed and provide a protective envelope for the electrode. Their structure and mechanism of formation, as well as the correlation between the surface chemistry, 3D structure, morphology, and the electrochemical behavior of the electrodes in solution, are discussed.

## Introduction

One of the most important advances in recent years in the field of energy storage and conversion relates to the development of Li ion batteries which are based on carbon−lithium insertion anodes, transition metal oxide−lithium intercalation cathodes, and electrolyte systems based on polar aprotic solvents or Li ion conducting polymers.

When a carbon electrode is polarized from open circuit voltage (OCV) to low potentials in organic polar aprotic solution containing lithium salts (3−2.5 → 0 V *vs* $Li/Li^+$), the following processes take place: below 2 V ($Li/Li^+$) the solution components, which include the solvent, the salt anion, and contaminants, are reduced.[1] The exact onset of these reactions depends on the specific species present in solution. The reduction of solvents from the alkyl carbonate, ether and ester families, commonly used salt anions (e.g. $ClO_4^-$, $AsF_6^-$, $PF_6^-$, $BF_4^-$, $N(SO_2CF_3)_2$), and atmospheric contaminants on carbon electrodes in the presence of Li cations form insoluble Li organic and inorganic salts, which precipitate on the electrode as surface films.[2] These Li salts, which precipitate as thin layers, are Li ion conductors, but also electronic insulators.[3] Thus, upon polarization, as the above reduction processes continue, these surface films reach a thickness that prevents electron tunneling through them. This stops the reduction of solution components and passivates the electrode (the SEI model[4]).

The chemical composition of these surface films, their physical structure, and, thus, their passivating ability and Li ion conductivity depend on a delicate balance between different surface reactions of the various solution components.[5,6] Thereby, in addition to the solution composition, the way in which the carbon electrode is polarized (e.g. galvanostatic, potential scanning, potential steps, low constant potential) also strongly influences the properties of these surface layers.[7] Parallel to these surface reactions, Li insertion processes also take place. The nature of these processes depends on the type of carbon. In the case of highly ordered, graphitic type carbons, the major Li insertion processes involve staged intercalation in which the Li ions diffuse between graphene planes. Layered, ordered Li−C intercalation compounds of a final stochiometry of $LiC_6$ are thus formed within a potential window between 0.25 and 0.01 V[8−10] ($Li/Li^+$). As the carbon has a less graphitic structure, its Li intercalation is more complicated and may occur within a larger potential window.[2,5,11]

In the case of disordered carbons, the Li insertion processes are very complicated and may include adsorption type interactions[12] and reactions with residual H−C bonds which may exist in carbons prepared from organic precursors at temperatures around 1000 °C.[13] In these cases, the potential window of Li insertion may be within 1.5−0 V ($Li/Li^+$).[12−14]

In most cases the onset potential of the above-described reduction processes of the solution components is higher than that of the Li insertion into the carbon, and thereby the latter process involves Li migration through the above-described surface films and may, in fact, be controlled by it. It was found that the reversibility and the capacity of Li insertion into carbons are strongly dependent on the composition of the electrolyte solution.[2,5,6,15] The more ordered and graphitic-like the carbon, the more pronounced the impact of the solution composition on the properties of the Li−C intercalation. It was suggested that the graphitic carbon may exfoliate due to coinsertion of solvent molecules with the migrating Li ions between graphene planes.[16] The common hypothesis is that in some cases of solution combinations, the above-described surface films are compact, protective, and effectively passivating, thus enabling only $Li^+$ migration, but preventing any coinsertion of solution species.[2,5,6,17] In other solution combinations, the structure of the surface layers and the way in which they precipitate cannot make them protective enough to prevent detrimental processes that cause deterioration of the graphite electrodes' capacity and reversibility during repeated intercalation with lithium. The results that emanate from different research groups concerning the stability of graphite electrodes in various electrolyte solution combinations are sometimes controversial, because many factors influence the complicated surface chemistry developed on the

[⊗] Abstract published in *Advance ACS Abstracts,* February 15, 1997.

S1089-5647(96)02815-5 CCC: $14.00 

electrodes. For instance, the presence of several tens of ppm of water, HF, and $CO_2$, which may be unavoidable in many electrolyte solutions, may considerably influence the chemical composition of the surface films developed on graphite and, consequently, the properties of the intercalation with lithium in terms of capacity, reversibility, stability, and interfacial resistance.[17−19]

Nevertheless, based on the intensive research of recent years, the following classification of electrolyte solutions for Li ion batteries emerges: binary solutions that contain ethylene carbonate (EC) and another cosolvent of lower viscosity, lower polarity, and a lower melting point, such as dimethyl diethyl or ethyl methyl carbonates[19,20] (DMC, DEC, EMC) or 2Me-THF,[21] especially with salts such as $LiAsF_6$ and $LiN(SO_2CF_3)_2$, are the best. Graphite electrodes can be cycled hundreds of times in these solutions, probably because of the highly protective and passivating properties of the surface films formed when the carbon surface chemistry is dominated by EC reduction. The behavior of graphite electrodes in $LiPF_6$ solutions of the above solvent mixtures depends on the level of HF contamination unavoidably present in these solutions.[22]

The presence of $CO_2$ further improves the cyclability of graphite electrodes because of the enrichment of the surface films with $Li_2CO_3$[2,5,6] (due to $CO_2$ reduction at low potentials). In contrast, graphite electrodes cannot be cycled in propylene carbonate (PC), tetrahydrofuran (THF), and $\gamma$-butyrolactone (BL) solutions.[2,5,6,23] A limited cyclability of graphite electrodes may be achieved in methylformate (MF),[2] 1,3-dioxolane,[3] and EMC single-solvent solutions, especially if the salt is $LiAsF_6$. There are also reports on chlorinated cyclic alkyl carbonates as good solvents for graphite electrodes.[24]

While it is now possible to map many solution combinations in connection with the reversibility, capacity, and stability of Li-graphite intercalation processes, the mechanisms of failure of graphite electrodes in "bad" solutions are not clear.

Questions such as why lithium intercalation into graphite in PC or THF is not reversible and what happens to the graphite's 3D structure in these cases are still unanswered. It is obvious that a better understanding of these issues is essential for the judicious optimization of electrode solutions for advanced Li ion batteries. This work presents an attempt to clarify and better understand the mechanisms of failure and stabilization of graphite electrodes upon intercalation with lithium in aprotic media. In particular, we chose to study THF solutions, as these are typical electrolyte systems in which Li−graphite insertion anodes seem to fail. On the other hand, because of the low to medium reactivity of this solvent at low potentials, the behavior of graphite electrodes may be pronouncedly influenced by additives, and thus understanding of this influence may contribute to a better understanding of stabilization and failure mechanisms of graphite electrodes in solutions. The electrolyte systems studied included dry THF, PC, THF−PC, wet THF, and EC−DMC solutions. The latter served as a reference system in which Li−graphite intercalation is highly reversible. Chronopotentiometry, impedance spectroscopy, and slow scan rate cyclic voltammetry, in conjunction with *in situ* and *ex situ* XRD, FTIR spectroscopy, and electron microscopy, were all applied.

## Experimental Section

THF, PC, EC, DMC, and $LiPF_6$ were obtained from Tomiyama (ultrapure, Li battery grade). $LiAsF_6$ was purchased from Lithco (L.B. grade). These chemicals could be used as received. The solution initially contained about 10−20 ppm $H_2O$ (by K.F. Titration, KF 562 Metrohm). Graphite particles were obtained from Lonza. The KS-series (75, 44, and 6 $\mu$m average particle size) was tested. Two types of carbon electrodes were prepared. Thick electrodes (100−200 $\mu$m thick) were prepared, as already reported,[2,5,6] using a copper grid (Exmet) current collector and PVDF binder (10%). Thin electrodes (8−9 $\mu$m thick) were prepared by depositing a coating made up of 90% graphite power (KS-6, Lonza) and 10% PVDF binder on a copper foil from a slurry of graphite particles and PVDF in 1-methyl-2-pyrrolidone. Li was obtained from Foote Minerals. The preparation of carbon electrodes for the spectroscopic measurements,[2,5,6] cycling carbon electrodes,[2,5,6,17] and the performance of *ex situ* FTIR,[2,5,6] SEM,[5] and impedance spectroscopy,[17] as well as the relevant instrumentation, were already described. There is, however, a change in the apparatus for FTIR measurements from that of previous work.[2,5,6,17] In the present measurements, the Magna 550 (Nicolet) FTIR spectrometer placed in a glovebox under $H_2O$- and $CO_2$-free atmosphere (compressed air treated by a Balston air purifier) was used.

A three-electrode cell was used for the electrochemical measurements (lithium counter and references electrodes). Cyclic voltammetric, chronopotentiometric, and chronoamperometric data were obtained, using an EG&G Model 273A potentiostat operated by Model 270 Research Electrochemical software, driven by an 486 IBM PC, or by using Schlumberger's 1286 electrochemical interface with Scribner (USA) software (486 IBM PC).

*In situ* XRD measurements were performed in a parallel plate polyethylene cell previously described.[19]

## Results and Discussion

Figure 1 presents eight chronopotentiograms ($V$ *vs* $t$ at constant current) measured with graphite electrodes in eight different 1 M $LiAsF_6$ solutions, as indicated, in similar experiments. The electrodes were discharged (Li intercalation) and charged (deintercalation) galvanostatically several times between 1.5 and 0 V ($Li/Li^+$), after which the potential was held constant close to 0 ($Li/Li^+$) for several hours, as indicated, followed by final galvanostatic deintercalation. The charge involved in this last step is also written near each graph, expressed in mole equivalents per $C_6$ ($Li_xC_6$). The initial electrode potential in each of these experiments was the open circuit potential close to 3 V ($Li/Li^+$). Figure 1a, which relates to the 1:1 EC−DMC mixture, may serve as a reference for the stable, reversible behavior of graphite−Li intercalation electrodes. The capacity of each cycle is close to optimum ($Li_{0.96}C_6$ *vs* $LiC_6$), and all the intercalation stages[25] are observed in the potentiogram.

In contrast, in dry THF solution (Figure 1b) it seems that in the first process some degree of Li intercalation takes place, but upon cycling, the capacity drops drastically. The final deintercalation step after prolonged polarization at low potential shows no capacity, which means that the electrode became inactive. In wet THF the behavior is different (Figure 1c), and while the capacity deteriorates from cycle to cycle, it is much higher compared with dry THF because the final deintercalation step involved about 76% of the electrode's full capacity. Hence, the decrease in capacity upon cycling should not be attributed to a drastic change in the active material, but rather to changes in the electrode's resistance. Indeed, as shown in Figure 1c, the potential jumps during the switch from intercalation to deintercalation (when the electrode's potential reaches the lower predetermined limit), which reflect the electrode's resistance, increase from cycle to cycle.

The behavior in THF solutions containing PC up to a certain concentration is somewhat similar to that observed in wet THF (Figure 1c). An optimum in reversible cycling and in the

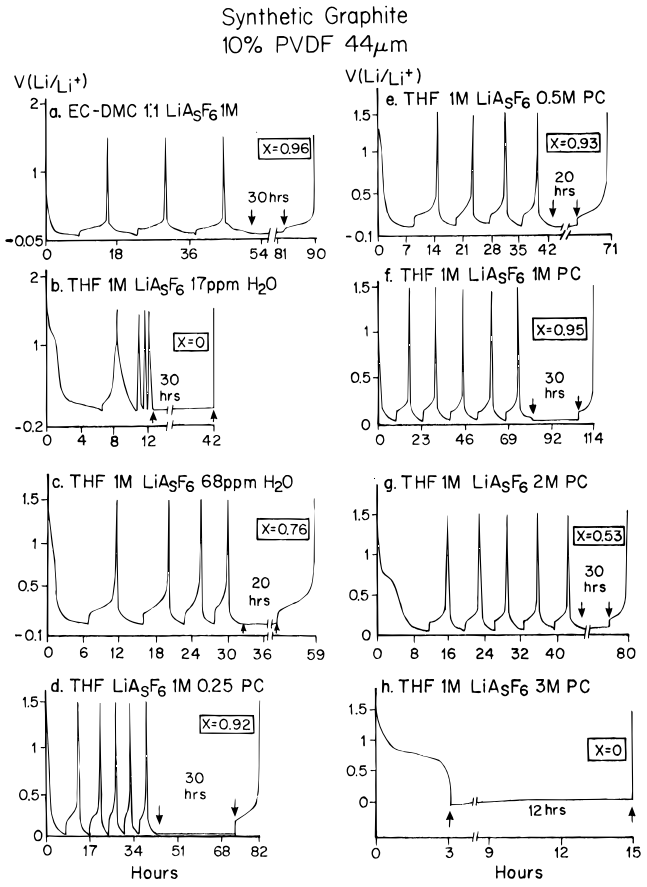


**Figure 1.** Chronopotentiometry (*V vs t*, constant current) of graphite electrodes (KS-44 Lonza, 10% PVDF) in various $LiAsF_6$ 1 M solutions. After a few cycles, as shown, the potential was held constant close to 0 V ($Li/Li^+$) for several hours (as indicated), followed by galvanostatic deintercalation. The charge involved in this last process expressed in molar equivalents per $C_6$ is marked. (a) 1:1 EC−DMC, (b) dry THF, (c) THF, 68 ppm $H_2O$, (d) THF 0.25 M PC, (e) THF 0.5 M PC, (f) THF 1 M PC, (g) THF 2 M PC, (h) THF 3 M PC.

electrode capacity ($X = 0.95$) is achieved with a solution containing 1 M PC (Figure 1f). When the PC concentration was 3 M, the behavior was similar to that observed in single-solvent PC solutions. The electrode could not reach all Li intercalation stages. The only process that could be seen (Figure 1h) relates to reduction of solution components (plateau between 1 and 0.5V). It should be noted that in all cases where the electrode capacity was medium to low or zero (dry THF, wet THF, 2 M and 3 M PC, Figure 1b, 1c, 1g,h, respectively), the initial electrode process, which involves reduction of solution species (1.5−0.5 V *vs* $Li/Li^+$), was much longer (more charge transfer) compared with the other cases in which the electrode capacity was high.

The following questions arose from these experiments: (1) Why is the electrode's capacity zero in dry THF or PC solutions, and is this related to major structural changes of the graphite (e.g. amorphization) or to surface phenomena? (2) How does the presence of $H_2O$ or PC in THF change the electrode's behavior so drastically? (3) What caused the observed deterioration of the electrode's capacity upon cycling in wet or PC-containing THF solutions?

The following results were obtained in an attempt to answer these questions.

Figure 2 presents voltammograms obtained with graphite electrodes in PC, THF, THF−$H_2O$, THF−PC, and EC−DMC solutions of $LiAsF_6$, as indicated. The potential was scanned from OCV (~3 V, $Li/Li^+$) to 0.3 V at 1 mV/s.

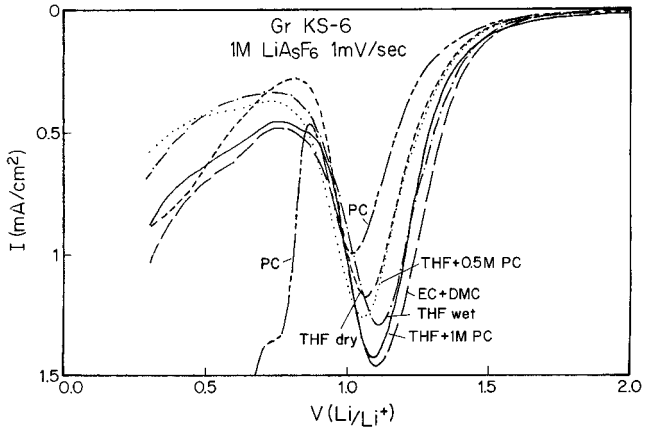


**Figure 2.** Linear sweep voltammograms obtained with graphite electrodes (KS-6 Lonza, 10% PVDF, 10 $\mu$m thick) in various $LiAsF_6$ 1 M solutions. The potential was swept from OCV (~3−2.5 V *vs* $Li/Li^+$) to 0.3 V at 1 mV/s. The various solution compositions are indicated near each curve.

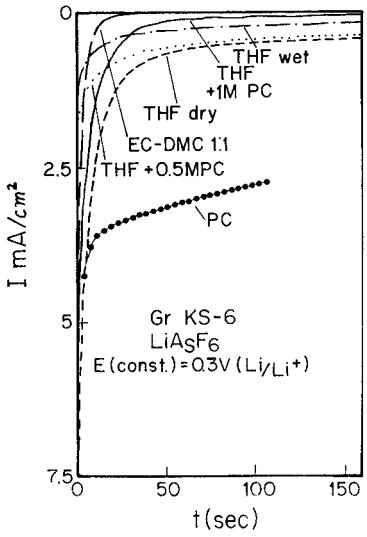


**Figure 3.** Chronoamperometry of graphite electrodes (KS-6, 10% PVDF, 10 $\mu$m thick) in various solutions as indicated. The potential was scanned from OCV (3−2.5 V *vs* $Li/Li^+$) to 0.3 V at 1 mV/s. The potential was then held constant, and the current *vs* time was recorded.

With all the above solutions, a pronounced peak was obtained around 1.1 V ($Li/Li^+$). Using $LiPF_6$/PC solutions in the same experiment, a peak around 1.8 V was obtained and no peak below 1.1 was recorded. The common species for all the solutions of Figure 2 is $LiAsF_6$. It is well-known that $AsF_6^-$ is reduced on noble metals to LiF and $AsF_3$ at potentials around 1.5 V in nonaqueous media.[26] Hence, we attribute the common peak around 1.1 V in Figure 2 to this process. The 1.8 V peak measured with the $LiPF_6$ solution should also be attributed to the reduction of the anion ($PF_6^-$). Indeed, recent EQCM studies of $LiPF_6$/PC solutions also indicate that this salt is reduced around 1.8−2 V ($Li/Li^+$).[27] As shown in Figure 2, as the potential was lowered, continuous reduction waves were recorded, attributable to the reduction of other solution components (e.g. solvent, contaminants). The very high currents measured below 0.8 V when the solvent was pure PC should be noted.

Figure 3 shows chronoamperograms which are, in fact, a continuation of the experiments described in Figure 2, obtained with graphite electrodes in the above solutions (indicated). The potential was scanned from OCV to 0.3 V ($Li/Li^+$), and the decay of the current was followed at this constant potential. With EC−DMC and 1 M PC−THF, solutions in which the Li−

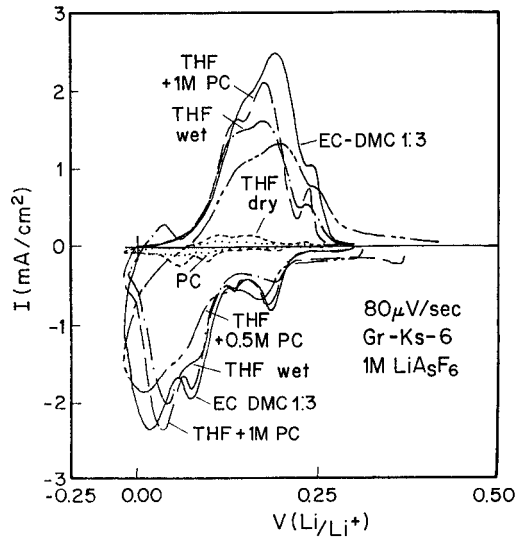


**Figure 4.** Cyclic voltammetry of graphite electrodes (KS-6, 10% PVDF, 10 $\mu$m thick) in the various solutions, as indicated, within the potential range of intercalation (0−0.25 V *vs* Li/Li$^+$). Scan rate of 80 $\mu$V/s.

**TABLE 1: Charge Involved in the Reduction of Solution Species on Graphite Electrodes in the Potential Domain OCV → 0.3 V (Li/Li$^+$) and Its Separation to Salt Reduction and Other Solution Component Reduction, as a Function of the Solution Composition ($LiAsF_6$ 1 M) (The Charges Are Expressed in Mole Equivalents per $C_6$)**

| solution | *Q* total | *Q* salt | *Q* other components |
|---|---|---|---|
| EC-DMC, 1:3 | 0.32 | 0.18 | 0.14 |
| dry THF | 0.9 | 0.19 | 0.71 |
| THF, 60 ppm $H_2O$ | 0.34 | 0.22 | 0.12 |
| THF, 1 M PC | 0.32 | 0.19 | 0.13 |
| PC | 0.95 | 0.12 | 0.83 |

graphite intercalation is the most reversible, the current decay is fast and the currents drop nearly to zero. This obviously indicates that the electrodes are efficiently passivated in these solutions.

In contrast, with PC and dry THF the currents are high and the decay is slow. In wet THF and 0.5 M PC−THF solutions, the behavior is of intermediate value between the above two cases. These combined chronopotentiometric, voltammetric, and chronoamperometric studies (Figures 1−3, respectively) enable the calculation of the charge involved in the formation of the surface films and its division between salt and other component's reduction as a function of the solution composition. The results are summarized in Table 1.

In THF and PC, the charge involved in reduction of solution species is the highest, and the percentage of the charge related to salt reduction is the lowest compared with the other solutions.

Figure 4 presents slow scan, first cycle voltammograms obtained from graphite electrodes in the above solutions, within the intercalation potential domain (after the potential was scanned from OCV). The three typical redox transfers around 0.225, 0.13, and 0.08V, diluted stage I (I(D)) ↔ stage IV, stage IV, III ↔ stage II, and stage II ↔ condensed stage I, respectively[8−10,28]) are observed. Since the scan rate was too high, 80 $\mu$V/s, the resolution of the various peaks was low. However, for the purpose of this presentation, which is to show the pronounced differences in the charge involved as a function of the solution studied, this peak resolution is sufficient.

These results converge nicely with those presented in Figure 1 and those obtained from chronopotentiometry. The highest electrode capacity was measured for EC−DMC and THF 1 M PC solutions (high currents). Very low electrode capacity was

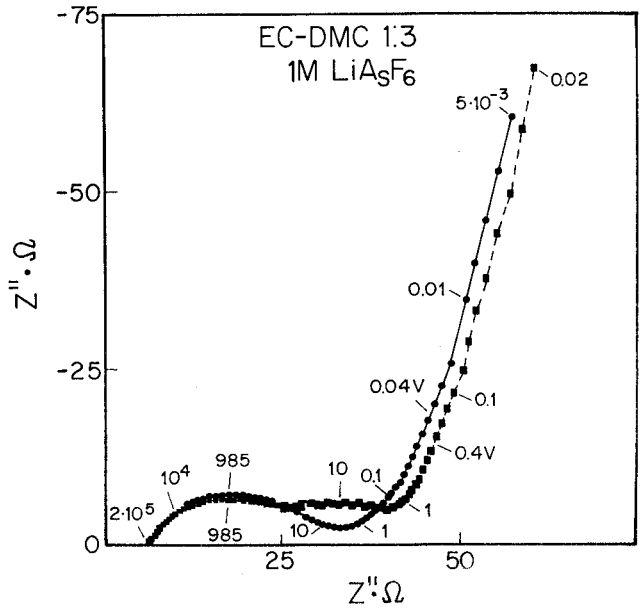


**Figure 5.** Nyquist plots measured from a graphite electrode at 0.4 and 0.04 V (equilibrium) in 1:3 EC−DMC, 1 M $LiAsF_6$ as indicated. The electrode was KS-6, 10% PVDF, 10 $\mu$m thick. Several frequency values are marked near each plot.

measured for dry THF and PC solutions, and the charges measured for wet THF and 0.5 M PC−THF solutions were of intermediate value between the high and the low ones. Hence, comparing Figures 3 and 4, there is a correlation between the charge involved in the intercalation processes and the degree of electrode passivation at the foot of the intercalation, as reflected by the decay in the currents at 0.3 V (good passivation ↔ high intercalation currents) and by the charge involved in the reduction of solution species (Table 1).

Figures 5−8 present results from impedance spectroscopic studies of thin (10 $\mu$m thick) graphite electrodes in the various solutions. Each measurement was performed at equilibrium potential (ac amplitude of about 1 mV), and the area of all the electrodes was the same (about 4.9 cm$^2$). For the purpose of this paper, the data are treated only qualitatively, since their major use was as a comparison of the electrodes' interfacial resistance. More quantitative and intense treatment of impedance spectroscopic data obtained from these systems is presented elsehwere.[29] Figure 5 shows Nyquist plots obtained with a graphite electrode in the reference solution 1:3, EC−DMC 1 M $LiAsF_6$ at two potentials: 0.4 V (Li/Li$^+$) at the foot of the intercalation, after the passivating surface films are well developed, and at 0.04 V, which is the potential of Li intercalation into phase I of the lithiated graphite.[8−10,25,28]

The Nyquist plot obtained at 0.4 V is characterized by a combination of two semicircles for the frequency range $10^5$−1 Hz. At lower frequencies, the plot is a sloping line, which becomes steeper as the frequency is lower. When the potential is 0.04 V only the semicircle of the high to medium frequencies ($10^5$−10 Hz) remains (Figure 5), and thus below 1 Hz, the plot becomes a sloping line. It should be noted that, despite the pronounced changes in the state of the electrode between the two potentials, as reflected by the Nyquist plots of Figure 5, the first, high to medium frequency semicircles of the two spectra are very similar in all their parameters ($Z''$, $Z'$, and frequency values). Based on previous studies of impedance spectroscopy of nonactive metal electrodes in aprotic media containing the same salt ($LiAsF_6$),[30] we attribute the high to medium frequency semicircle in these spectra to the surface films that cover the electrode. Thus, the diameter of this

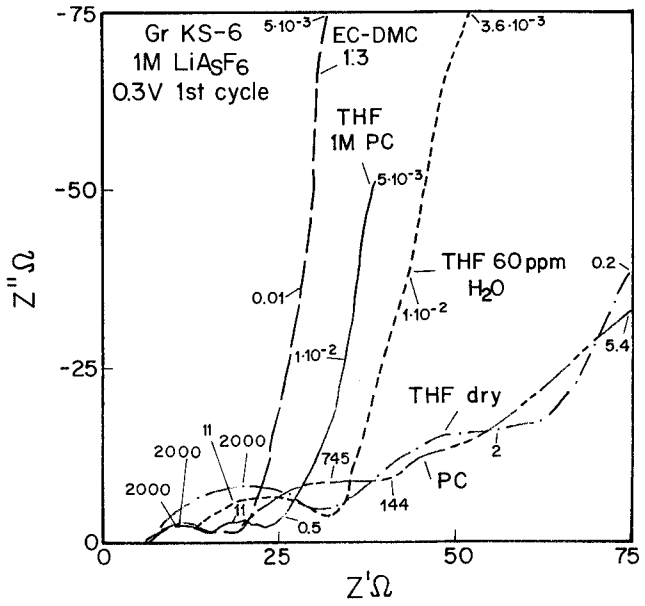


**Figure 6.** Impedance spectra (Nyquist plots) measured from graphite electrodes in the various 1 M $LiAsF_6$ solutions as indicated (KS-6, 10% PVDF, 10 $\mu$m thick). The electrodes were measured at equilibrium at 0.3 V ($Li/Li^+$) after the surface reactions related to the solution components were completed. The ac amplitude was 1 mV around equilibrium. Various frequency values are marked near each plot.

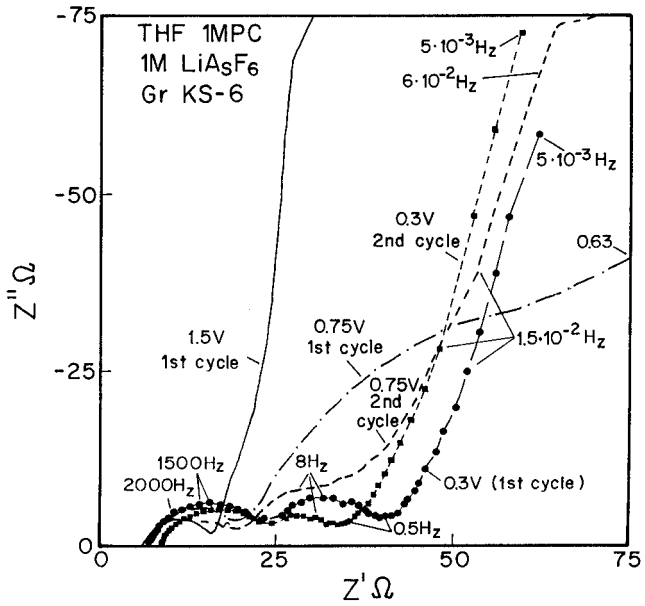


**Figure 7.** Nyquist plots measured from a graphite electrode (KS-6, 10% PVDF, 10 $\mu$m thick) in a THF/1 M $LiAsF_6$/1 M PC solution at different potentials during the first and second intercalation process, as indicated. Several frequency values are marked near each plot. The electrode reached complete equilibrium before each measurement, and the ac amplitude was 1 mV around the equilibrium potential.

semicircle roughly reflects the resistance to $Li^+$ migration through the films[30] and is on the order of 100−200 $\Omega\cdot cm^2$ (depending on the electrode's thickness), which is on the order of magnitude of the interfacial resistance of Li electrodes in the same solutions.[17,22] Indeed, Li and graphite at low potentials in EC−DMC mixtures are covered with surface films of similar composition.[22] The capacity calculated for this semicircle is on the order of a few $\mu F/cm^2$, which is also typical of these surface films's capacitance.[30] It is anticipated that the surface films formed on graphite in EC−DMC $LiAsF_6$ solutions do not change as a function of the electrode potential because, once they are formed and precipitated at potentials above 0.4 V, they are very stable. This is, in fact, the main reason for the high stability and reversibility of graphite−Li intercalation anodes in these electrolyte solutions.[22]

The low-frequency part of the spectra of Figure 5 relates to the redox behavior of the electrode and to $Li^+$ diffusion in both solution and graphite phases.[29] (Part of the sloping lines in Figure 5 should be assigned as "Warburg" type elements.[29]) At the lowest frequencies the electrode approaches pure, capacitive behavior. In contrast to the impedance related to the surface films covering the electrode, the impedance part which reflects the redox behavior of the electrode is expected to be strongly dependent on the potential applied, which is, indeed, in agreement with the changes in the second semicircle observed in Figure 5.

Figure 6 presents Nyquist plots obtained with graphite electrodes polarized to 0.3 V ($Li/Li^+$, at the foot of the intercalation with Li) in five solutions, as indicated. It should be noted that the spectra measured with EC−DMC, wet THF, and THF/1 M PC solutions have a similar structure, as discussed above. The changes observed among them are mostly in the second, low-frequency semicircles, which differ in size from system to system. The plots relating to PC and dry THF solutions are remarkably different from those of the other three solutions and reflect much higher interfacial resistance, as demonstrated in Figure 6. The fact that these two spectra differ from the other three along the entire frequency range, including very low frequencies, indicates that there are pronounced structural differences between graphite electrodes polarized in THF or PC solutions and those polarized in solutions such as EC−DMC, wet THF, or THF/low-concentration PC, in which these electrodes behave reversibly upon intercalation with lithium.

Figure 7 presents Nyquist plots obtained from a graphite electrode in 1 M $LiAsF_6$/1 M PC/THF solution at various potentials above the onset of the intercalation during a first and a second consecutive polarization from OCV to 0 V ($Li/Li^+$). Pronounced changes are observed between spectra measured at the same potential but at different cycles, mostly at the low frequencies. Although the major solution reduction processes that form the surface films occur in this solution below 1.5 V (see Figure 2), the Nyquist plot obtained at 1.5 V includes a high-frequency semicircle which is attributed to surface films (in addition to a steep, sloping line at the low frequencies, which mostly reflects a capacitive behavior). This probably indicates that surface films are formed at potentials higher than those of the plateaus or the peaks in Figures 1 and 2 (respectively). There are indeed solution species such as trace $O_2$ and even trace $H_2O$ that can be reduced on these electrodes to insoluble $Li_2O$ or LiOH at potentials higher than 1.5 V.[30] The major difference between the first and the second cycles in these experiments is that during the first cycle the surface films are formed and stabilized at the potential range OCV → 0 V ($Li/Li^+$). During the second cycle, these surface films are fully developed and stable in the case of THF/1 M PC/1 M $LiAsF_6$ solution. Thus, only the spectra related to the second cycle in Figure 7 reflect a stable graphite electrode. It should be noted that the diameter of the second, low-frequency semicircle appearing in the Nyquist plots meausred during the second intercalation cycle is smaller than that in the Nyquist plot measured during the first cycle. This means that the organization of these electrodes taking place during the first intercalation cycle (surface film formation and their stabilization, etc.) reduces their charge transfer resistance. Figure 8 presents Nyquist plots obtained with a graphite electrode in wet (60 ppm $H_2O$) THF/$LiAsF_6$ 1 M solution at 0.3 V (close to the onset of the intercalation) and at 0.005 V (a fully intercalated electrode). The basic similarity between these

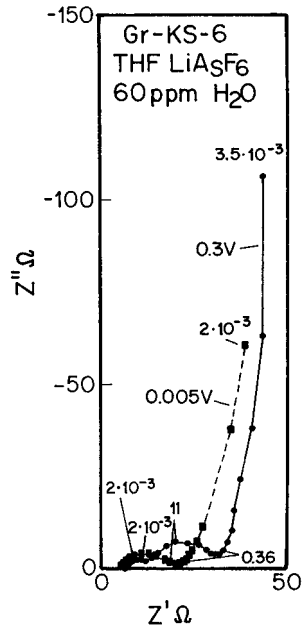


**Figure 8.** Same as for Figure 7. Nyquist plots measured at two potentials as indicated. Before and during intercalation. A THF $LiAsF_6$ 1 M solution containing 60 ppm $H_2O$.

**TABLE 2: Resistance and Capacitance of Graphite Electrodes Related to the First and Second Semicircles of the Nyquist Plots Appearing in Figures 5−8, Calculated for the Various Solutions (Electrode Area = 4.9 cm$^2$; The Separation of the Relevant Time Constants and the Calculations Were Made Using the Zview Program (Scribner), As Already Reported[30])**

| | high to medium frequencies first semicircle Li migration and surface films and film capacitance | | low frequencies second semicircle porous part of the surface films and charge transfer | |
|---|---|---|---|---|
| solution ($LiAsF_6$) | $R$ (Ω) | $C$ ($\mu$F) | $R$ (Ω) | $C$ ($\mu$F) |
| EC−DMC, 1:3 | 8.9 | 6.8 | 8.4 | 1300 |
| 1 M PC/THF | 10.6 | 4.5 | 10.1 | 1200 |
| THF, 60 ppm $H_2O$ | 10.4 | 9.3 | 23.5 | 670 |
| dry THF | 27.5 | 2.3 | 58 | 1600 |
| PC | 29.6 | 6.5 | 556 | − |

spectra and those of Figure 5, which were measured from completely different solutions but at similar states of the electrode, is very interesting.

A major, significant conclusion from these impedance spectroscopic studies is that reversible and stable Li−graphite intercalation anodes in quite different solutions *have similar* characteristic Nyquist plots. A high-frequency semicircle reflects the resistance and the capacity of the surface films (100−200 Ω·cm$^2$, a few $\mu$F/cm$^2$, respectively), and a low-frequency semicircle appears at potentials close to the onset of the Li intercalation (0.5−0.25 V *vs* Li/Li$^+$), which probably relates to the charge transfer behavior of these electrodes and their porous structure. We attribute this second semicircle to charge transfer with solution species, which occurs to a limited extent through the surface films (similar to the behavior of nonactive electrodes in these solutions[30]). The $R_{ct}$ calculated from the diameter of this semicircle is also around 100−200 Ω·cm$^2$ and is potential dependent,[29] but the relevant capacitance is on the millifarad scale. Since the graphite electrodes used in these measurements are thin and the graphite particles are not porous, these high-capacity values cannot be attributed to high electrode porosity.

In our previous work,[30] it was concluded that the surface films formed on Li or noble metals in these solutions are highly porous and thus have a high surface area in their outer, solution side. Therefore, impedance spectra measured from noble metal electrodes polarized to low potential in these solutions always include time constants of high capacitances which are attributed to the outer part of the surface films that cover the electrodes, coupled with charge transfer with solution species.[30] Hence, the second, low-frequency semicircle in the spectra of Figures 5−8 is assigned accordingly. Table 2 summarizes the $R$ and $C$ values calculated from the semicircles appearing in the Nyquist plots obtained from these electrodes at the foot of Li intercalation (0.3 V *vs* Li/Li$^+$). The data in this table demonstrate the pronounced difference in the electrode's resistance in dry THF and PC compared with the other solutions.

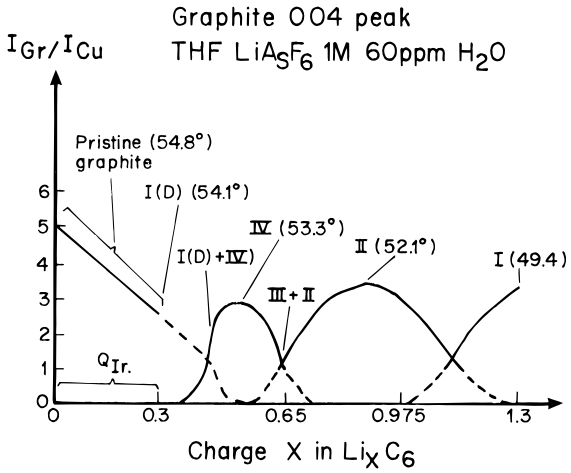


**Figure 9.** Summary of *in situ* XRD measurements of a graphite electrode (100−200 $\mu$m thick, KS-6, 10% PVDF) in THF $LiAsF_6$ 1 M solution containing about 60 ppm of $H_2O$. The relative intensity of the 004 peak (compared with the XRD peak of Cu at 2$\theta$ of 50.4°) is plotted as a function of the charge involved. The relevant peak's scattering angle and the Li-graphite phases involved are marked (I(D) corresponds to diluted stage I). The XRD patterns were measured during slow (C/20 h) galvanostatic charging (intercalation). The radiation source was Cu K$\alpha$.

The behavior of graphite electrodes in THF and PC solutions was also investigated using *in situ* and *ex situ* XRD, following changes in the 002 and 004 peaks of graphite. In EC−DMC, low-concentration PC in THF, and wet THF solutions, all the intercalation stages are observed, as reflected by the appropriate shifts of the above peaks.[18−10,25,28]

Figure 9 summarizes typical *in situ* XRD measurements of a graphite electrode in wet (60 ppm $H_2O$) $LiAsF_6$ 1 M THF solution. The electrode was slowly polarized galvanostatically (a full capacity during 20 h, C/20 h), and XRD patterns were measured repeatedly (about 5 min per measurement). The relative intensity of the 004 graphite peak and the copper peak from the electrode's grid (used as an internal standard) is plotted as a function of the charge involved, expressed in mole equivalents per $C_6$. The relevant scattering angle values (Cu K$\alpha$ radiation source) and the various Li−graphite phases formed during the intercalation processes are also marked. The domains of a coexistence of two phases (dashed lines) are also indicated. The significance of this presentation is that a complete intercalation between Li and graphite through all the relevant stages occurs in wet THF solutions. In contrast, Li intercalation is not observed by the XRD measurements in dry THF and PC solutions.

Figure 10 presents the changes in the electrode potential during slow galvanostatic polarization (C/20 h about 0.2 mA/cm$^2$) and the relative intensity of the 004 XRD graphite peaks measured *in situ* as a function of the charge injected into the electrode in PC $LiAsF_6$ solutions. The electrode in these

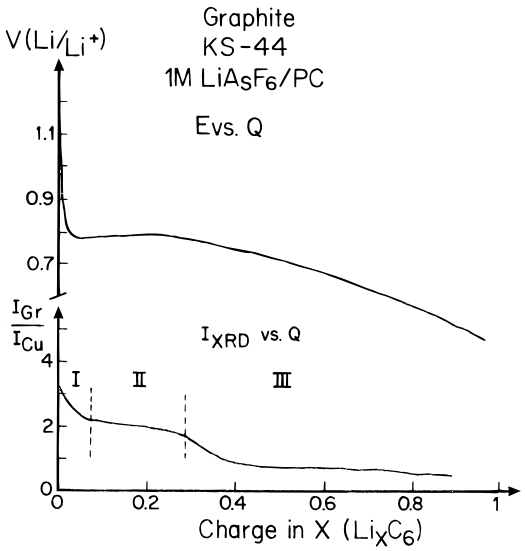


**Figure 10.** Typical chronopotentiometric response and the relative intensity of the 004 XRD peak of graphite (compared with that of the neighboring Cu XRD peak at $2\theta = 50.4°$) measured during *in situ* experiments with a KS-44, 10% PVDF, 100−200 $\mu$m thick electrode, in a PC $LiAsF_6$ solution. $E$ and $I_{graphite}/I_{Cu}$ (XRD) are plotted *vs* the charge involved, expressed as molar equivalents per $C_6$ (constant current). The current density was about 0.5 mA/cm$^2$ (∼C/20 h). The XRD 004 peak was measured repeatedly during the experiment (about 5 min per a complete data collection).

experiments consisted of graphite particles of about 44 $\mu$m average size. Electrodes comprising particles of 6 and 75 $\mu$m average size were also studied. While the behavior observed for these electrodes basically resembles that shown in Figure 10, the shape of both graphs $E$ vs $Q$ and $I_{XRD}$ *vs* $Q$ depends to a small extent on the graphite particle size.

At the beginning of the experiment during the injection of about 0.1 molar equiv per $C_6$ (salt reduction processes, Figure 2 and related discussion), there is a pronounced decrease in both the potential and the XRD peak intensity (region I, Figure 10). During continuous charge injection (PC reduction) up to about 0.3 molar equiv per $C_6$, a slight increase is seen in the potential, while the XRD peak intensity does not change (region II, the plateau in Figure 10). Further charge injection causes a decrease of the potential and the XRD peak intensity, as shown in Figure 10 (region III), and no shift in the peaks is observed (in contrast to cases where intercalation with Li occurs). After a charge injection of about 0.9−1 molar equiv per $C_6$, the surface reactions come to completion, the potential drops to Li deposition values (see Figure 1), and the XRD peak intensity then recorded is about 10% of its initial value. Such behavior is in agreement with the assumption that the graphite particles exfoliate in these solutions upon charging and come to a partial amorphization, as suggested in previous papers.[16,19] However, when the carbon material of these electrodes was measured after the experiments in PC solutions, *ex situ* by XRD (powdered and dried), the XRD pattern was typical of graphite and similar to that of the pristine material.

Thus, the decrease in the XRD peaks usually observed in the *in situ* XRD measurements[19] is not because of a completed amorphization of the graphite but, rather, is due also to optical and orientation changes that occur during polarization of the graphite electrodes in PC or THF solutions. In separate experiments, graphite electrodes were measured dry in the cell for *in situ* XRD measurements, and then a PC solution was introduced into the cell and no electrochemical process was conducted. A pronounced decrease in the graphite peaks' intensity was observed just due to the presence of the solution. Hence, we can attribute the pronounced decrease in the XRD peak intensity shown in region I of Figure 10, at least in part, to the absorption of the X-ray beam by solvent molecules trapped in the electrode's pores and within partially exfoliated graphite. The increase in the potential in region II of Figure 10 is attributed to an increase of the surface area of the electrode, which decreases its interfacial resistance. Hence, this may be indicative of some exfoliation of the graphite that takes place as PC reduction becomes the dominant surface reaction.

Figure 11 presents eight SEM micrographs obtained from graphite electrodes. Figure 11a was obtained from a *typical* pristine electrode with highly oriented graphite platelets whose basal planes are oriented horizontally (parallel to the current collector). Figure 11b is from a pristine disoriented electrode prepared by spreading the graphite/PVDF slurry on the current collector without giving any orientation (by pressure) to the platelets. The electrodes for micrographs 11c-h were identically prepared (highly oriented graphite platelets), treated and measured. These thin graphite electrodes (about 12−10 $\mu$m thick, average particle size about 6 $\mu$m) were galvanostatically polarized from OCV (3 V) to 0 V (Li/Li$^+$) and back to OCV in THF 1 M PC (11c), dry THF (11d,e), PC (11f,g), and wet THF (60 ppm $H_2O$, 11h), $LiAsF_6$ 1 M solutions. While in the pristine electrodes the graphite platelets are organized on the copper foil with their wide dimension facing upward, as shown in micrograph 11a, after being treated in PC or dry THF, the electrode structure became disordered. (micrographs 11d−g, compare with 11b). A pronounced change in the platelet orientation was observed, but the particles remained basically integrated. In contrast, the electrodes treated in THF 1 M PC (11c) or wet THF solutions (11h) retained their ordered structure, which remained similar to that of the pristine electrodes. These combined XRD and SEM studies reveal that the failure mechanism of graphite electrodes in PC and dry THF solutions is not due to a complete exfoliation and amorphization of the graphite particles, because of coinsertion of solvent molecules into graphite by intercalating Li ions at low potentials, as was proposed in previous papers,[2,5,6,16,19] but rather involves structural changes in the electrodes at a more macroscopic level occurring at solvent reduction potentials. Surface processes that take place as solution components are reduced at potential much above the intercalation onset change the electrodes' structure, separate the particles from each other, and change their orientation. We assume that this change in orientation also contributes to the pronounced decrease in the intensity of the XRD peaks observed during *in situ* measurements in PC or THF solutions (in addition to the absorption of cointercalated solvent molecules mentioned above). Hence, we assume that detrimental processes that exacerbate the electrodes' capacity in these solutions take place also outside, around the particles. Graphite particles may be disconnected electrically from the bulk in a manner very similar to that in which Li dendrites are disconnected electrically from the mother electrode by formation of insulating surface layers around them. The question is how these processes start. In answering this question, two points have to be considered. The poor performance of carbon−Li intercalation anodes in PC and THF solutions is unique to layered, graphite carbons. Disordered carbons and even graphitic carbons with some turbostratic disorder can be cycled in PC solutions.[2,3,8−10,16,23] In addition, in contrast to graphite electrodes, both lithium and nonactive metal electrodes at low potentials are efficiently passivated in PC and THF solutions.[27,30−33] The lack of passivation of graphite electrodes in these solutions, as well as the pronounced interfacial resistance measured, leads to the conclusion that reduction of

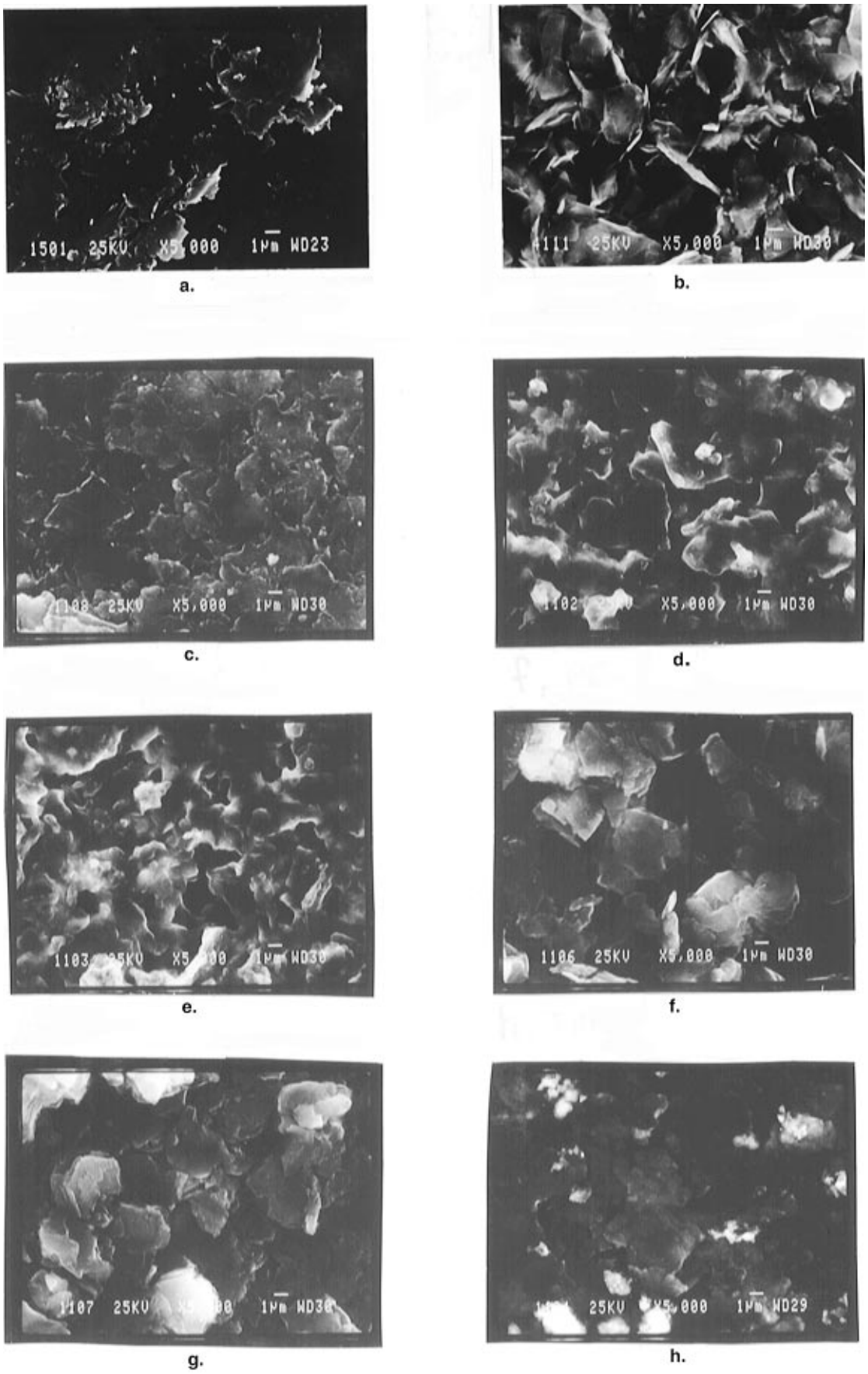


**Figure 11.** SEM micrographs obtained from pristine graphite electrodes and from highly oriented electrodes after being cycled in various $LiAsF_6$ 1 M solutions (KS-6, 10% PVDF, 10 $\mu$m thick). A scale appears in each picture. (a) Pristine electrode before the electrochemical treatment, highly oriented. The basal planes of the graphite platelets are oriented horizontally; (b) pristine electrode, disoriented; the graphite platelets are bound in disorder; (c) THF 1 M PC solution; (d,e) dry THF solutions; (f,g) PC solutions; (h) THF solution containing 60 ppm of water.

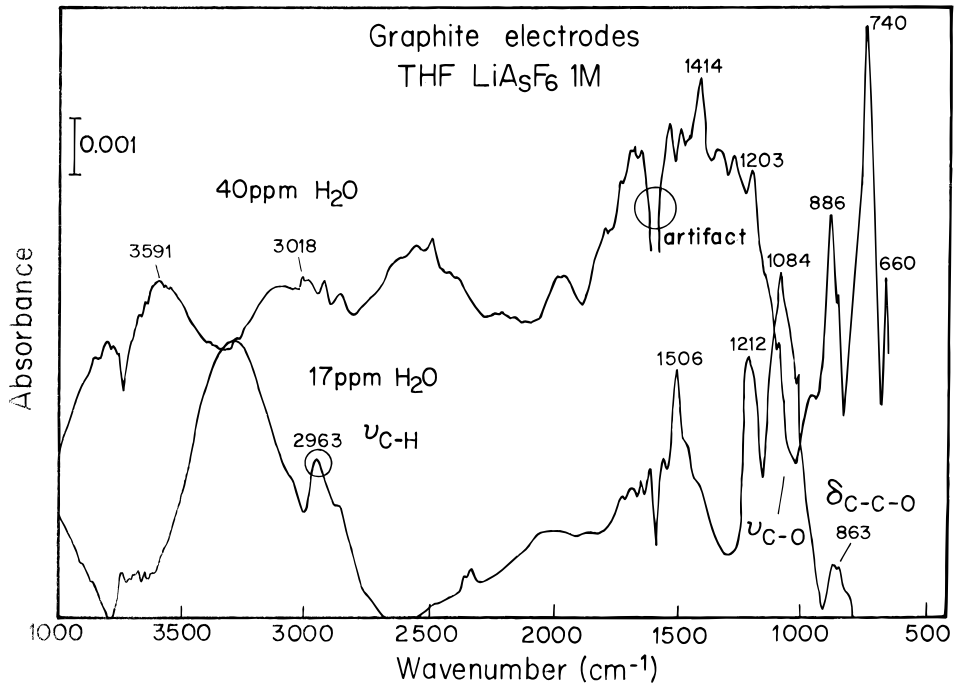


**Figure 12.** FTIR spectra measured using diffuse reflectance mode from graphite particles taken from electrodes after being cycled in THF $LiAsF_6$ solutions. Partial peak assignment appears. (a) Dry solution, (b) solution containing about 40−50 ppm $H_2O$.

PC and THF on layered graphitic carbon involves a considerable change in the electrodes' surface area during the process, which prevents precipitation of stable compact surface layers (Figure 10, region II and related discussion).

We conclude that reduction of PC and THF molecules on the edges of the graphite planes, even at potentials above the onset of massive lithium intercalation, causes some exfoliation of the graphite because of some possible intercalation of solvent molecules and volume difference between the inserted solvent molecules and their reduction products, which are Li salts and gases (e.g. propylene[2,5]). This exfoliation takes place mostly on a microscopic level, on the graphite surface. This is in agreement with the massive surface reactions taking place and the formation of resistive surface layers. Because layered graphite can be so easily peeled off and split, this micro-exfoliation initiates cracks that split the graphite particles macroscopically and enable more solvent molecules to diffuse into these cracks and to be reduced, and thus the structure of the electrode changes. Graphite particles are lifted up and electrically isolated from the bulk. This scenario is relevant only to *layered* graphite material in which surface reactions and microexfoliation can initiate cracks and splitting, and to solutions in which the surface reactions do not passivate the electrodes quickly enough (depending on the specific nature of the reduction products).

Another important point that should be discussed is how the presence of $H_2O$ and PC stabilizes the graphite electrodes and improves their performance. Surface sensitive FTIR spectroscopy was applied in diffuse reflectance mode for the study of the carbon surface layers covering the carbon particles after the electrodes were cycled in solutions. The spectra obtained from such measurements are usually not of high quality, but nevertheless are conclusive.

Figure 12 compares the spectra obtained from graphite particles after cycling in dry (12a) and wet (40−50 ppm, 12b) THF 1 M $LiAsF_6$ solutions. Spectrum 12a has pronounced peaks around 2963 $cm^{-1}$ ($\nu_{C-H}$), 1500 $cm^{-1}$ (graphite vibration), 1200 $cm^{-1}$ ($\nu_{C-F}$ PVDF binder), 1080 $cm^{-1}$ ($\nu_{C-O}$), and 860 $cm^{-1}$ ($\delta_{C-C-O}$ in this case). On the basis of our previous

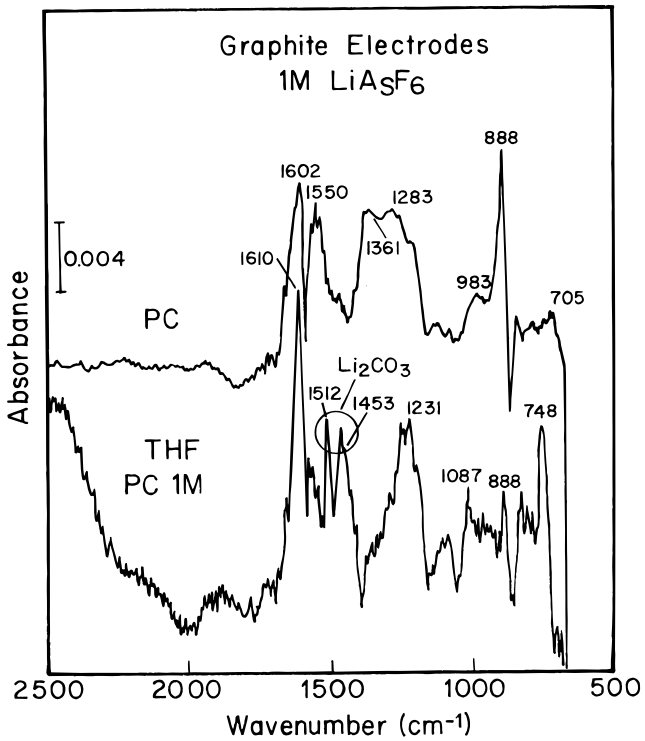


**Figure 13.** Same as for Figure 12. (a) PC solution, (b) THF 1 M PC solution.

studies[5,6,17,22,31] we concluded that this spectrum mostly reflects reduction of THF to Li alkoxy (ROLi) species on the graphite surface. Spectrum 12b related to the wet solution lacks the pronounced $\nu_{C-H}$ and $\nu_{C-O}$ peaks. This spectrum also does not have any peaks of the expected $H_2O$ reduction product LiOH, indicating that $H_2O$ may be reduced further to $Li_2O$ as the final product. $Li_2O$ has a pronounced IR band around 600 $cm^{-1}$ and thus cannot be detected by these measurements because of the use of the MCT detector in the FTIR spectrometer.

We conclude that the formation of an oxide layer suppresses competing solvent reduction on the surface. As already known

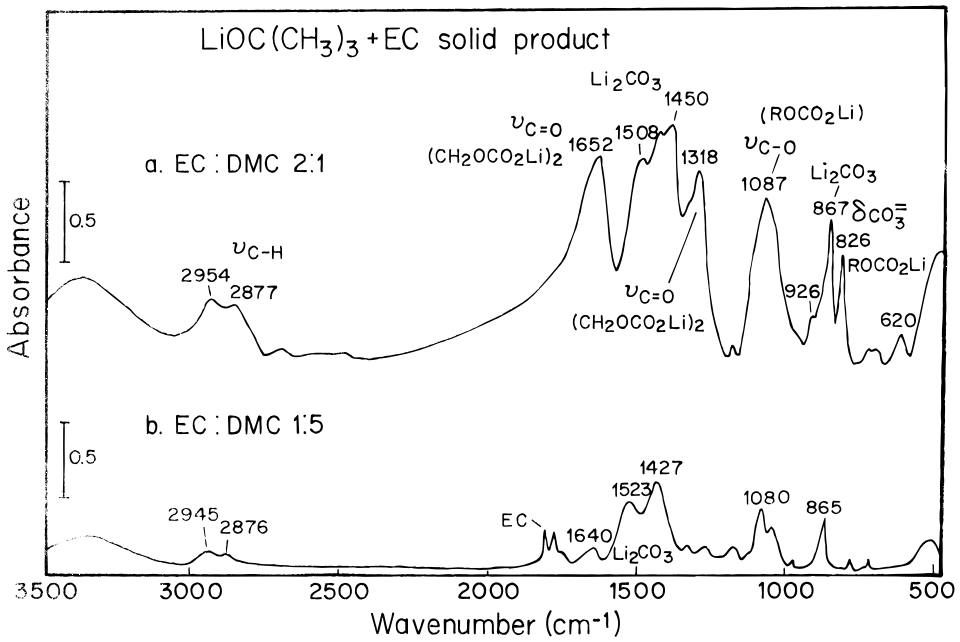


**Figure 14.** FTIR spectra of the solid products precipitating in reactions between $LiOC(CH_3)_3$ and EC in DMC solutions. These products were measured, pelletized in KBr (transmittance mode). (a) 2:1 EC−DMC, (b) 1:5 EC−DMC. The concentration of the reacting nucleophile in solution was about 1 M.

from previous studes,[32] $Li_2O$ films better passivate Li and nonactive metal electrodes at low potentials than Li organic salts such as ROLi. Hence, the improvement in the performance of graphite electrodes achieved in wet THF solutions should be attributed to the formation of surface Li oxide, which precipitates as a protective cover on the electrode and thus prevents massive solvent reduction. Figure 13 presents FTIR spectra measured from graphite particles from electrodes treated in PC and THF 1 M PC solutions (a, b, respectively). These spectra are quite different from those of Figure 12. Spectrum 13a has a pronounced broad peak between 1700 and 1500 $cm^{-1}$, a broad band between 1380 and 1150 $cm^{-1}$, small peaks around 1100−1000 $cm^{-1}$, a pronounced peak around 880 $cm^{-1}$, and small peaks around 820 and 700 $cm^{-1}$. PC is reduced on Li and noble metal electrodes at low potentials to $ROCO_2Li$ species, whose most pronounced absorption in the IR is the carbonyl peak around 1650 $cm^{-1}$ ($\nu_{C=O,as}$).[31−33] We thereby attribute the pronounced peak around 1600−1650 $cm^{-1}$ in spectrum 13a to these species. The broad band around 1380−1150 $cm^{-1}$ may be a combination of several absorptions, including $\nu_{C=O,S}$ around 1300 $cm^{-1}$ [31−33] and $\nu_{C-F}$ around 1200 $cm^{-1}$. The $ROCO_2Li$ species also have peaks around 1100 $cm^{-2}$ ($\nu_{C-O}$) and 820 $cm^{-1}$ ($\delta_{CO3^{2-}}$). At this moment we cannot assign the strong 888 $cm^{-1}$ peak in spectrum 13a. Both $Li_2CO_3$ and several alkoxy species have pronounced peaks between 890 and 870 $cm^{-1}$. However, this peak cannot be assigned as a $Li_2CO_3$ peak because this has its pronounced IR band around 1500−1450 $cm^{-1}$, which is absent in Figure 13a. Spectrum 13b is quite different from both spectra 13a (PC) and 12a (dry THF). It has pronounced peaks around 1610 $cm^{-1}$ (assigned to $\nu_{C=O,as}$ of $ROCO_2Li$), 1510−1450 $cm^{-1}$ (assigned as a superposition of $Li_2CO_3$ and $\delta_{CH_2,CH_3}$ peaks), 1300 and 1200 $cm^{-1}$ ($\nu_{C=O,S}$, $ROCO_2Li$ and $\nu_{C-F}$, PVDF), 1090 $cm^{-1}$ ($\nu_{C-O}$, $ROCO_2Li$), 1000 $cm^{-1}$ ($\nu_{C-O}$, ROLi), and 880 $cm^{-1}$. The latter peak may be attributed to $Li_2CO_3$, as the other pronounced band of $Li_2CO_3$ also appears in this spectrum. These spectral results seem to indicate that the surface films formed on graphite in THF/PC 1 M comprise a combination of $ROCO_2Li$, which is a major PC reduction product, and $Li_2CO_3$ and ROLi species, products of THF reduction.

It is well-known that $Li_2CO_3$ is one of the best passivating agents for both lithium and graphite electrodes.[2,5,6,17,33] It is logical to assume that the stability of graphite electrodes and their improved performance in THF solutions containing a low concentration of PC are due to the formation of surface $Li_2CO_3$, which improves the passivating and protecting properties of the surface layers. The question is why $Li_2CO_3$ is formed on the surface when the PC concentration in solution is low, while in PC solutions the major surface species formed are $ROCO_2Li$ compounds.[30−33]

In a parallel investigation, we explored reactions between ethylene carbonate (EC) and nucleophiles such as lithium *tert*-butoxide in order to simulate possible reduction paths of this important solvent on electrode surfaces. As already proven, EC and PC are reduced on active electrodes in a very similar manner in terms of mechanisms and product distribution.[33] When Li *tert*-butoxide ($LiOC(CH_3)_3$) is dissolved in EC−DMC mixtures, solid products may be isolated and identified.

Figure 14 presents FTIR spectra of the solid products between Li *tert*-butoxide and EC in 2:1 EC−DMC and 1:5 EC−DMC mixtures (14a,b, respectively). Surprisingly, spectrum 14 is identical to the spectrum of the combination of $Li_2CO_3$ and $(CH_2OCO_2Li)_2$, which is the major reduction product of EC on Li and carbon.[17,22,33] The NMR spectrum of this solid, dissolved in $D_2O$, has the typical singlet of the $-OCH_2CH_2O-$ group[33] as its *major* peak. In spectrum 14b the dominant peaks belong to $Li_2CO_3$ (1520−1430, 865 $cm^{-1}$). The only way to explain the formation of lithium ethylene dicarbonate in this case is by a nucleophilic attack of inorganic carbonate $CO_3^{2-}$ on EC molecules, as shown in Scheme 1. Hence, the product distribution reflected by the spectra of Figure 14 may be explained as follows: nucleophilic attacks on both carbons of the EC molecule form $CO_3^{2-}$ or $LiCO_3^-$, which may be nucleophiles when unpaired with $Li^+$. These anions may either attack another EC molecule to form ethylene dicarbonate or, being paired by Li ions, precipitate as insoluble $Li_2CO_3$. In this state, $Li_2CO_3$ is not a nucleophile at all because of the strong interaction between the $Li^+$ and the carbonate anion, which makes it so insoluble in these systems. Hence, the product distribution should depend on the concentration of the electrophile, EC.

**SCHEME 1: EC (PC) Reduction Mechanisms**

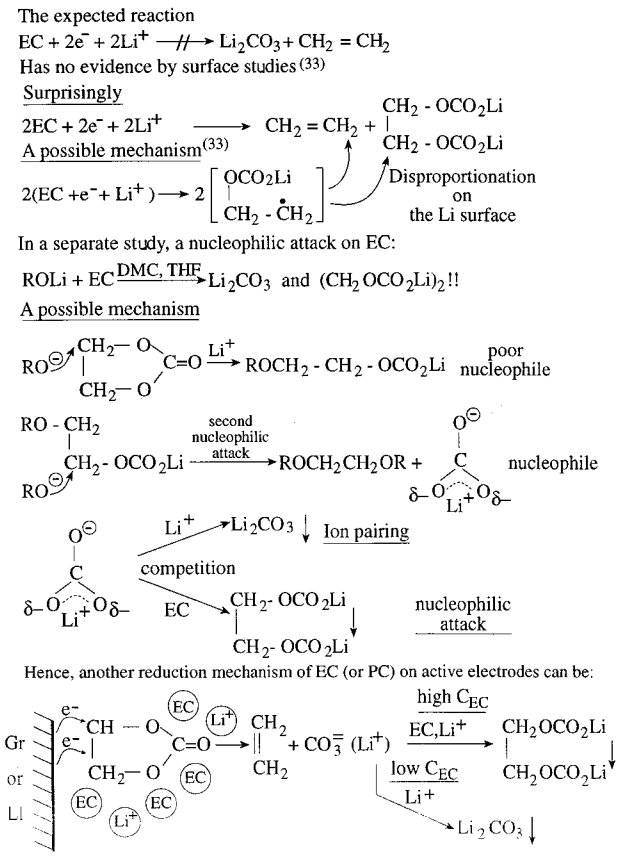


Thus, at high EC concentration (Figure 14a), $(CH_2OCO_2Li)_2$ is a major product, while at low EC concentration, $Li^+$ competes successfully with EC as electrophiles for the carbonate anion, and thus $Li_2CO_3$ is the major product (Figure 14b).

On the basis of this study, as illustrated in Scheme 1, we suggest a reaction path in which nucleophilic attack of an unpaired carbonate anion on solvent molecules is involved as one of the possible mechanisms for EC or PC reduction on active surfaces in the presence of Li ions. In both cases, alkylene dicarbonate is the major surface species formed (in addition to alkylene gas).[33] Thus, it is quite possible that both molecules undergo near reducing active surfaces two-electron transfer to form the corresponding alkylene gas molecules and active, nucleophilic $CO_3^{2-}$ or $LiCO_3^-$ (coupling with one $Li^+$). These attack neighboring solvent molecules nucleophilically to form $ROCO_2^-$ species, which precipitate with $Li^+$ to form the observed $ROCO_2Li$ products (see Scheme 1). The behavior of graphite electrodes in THF solutions containing low concentration of PC solutions may thus be well understood. When PC is reduced on the active carbon surface and a nucleophilic, solution carbonate is thus formed, the relatively low PC concentration allows precipitation of this solution carbonate as $Li_2CO_3$. As the PC concentration increases, the product distribution shifts more and more toward the formation of the much less protective and passivating $ROCO_2Li$ species (Li propylene dicarbonate in the case of PC). Thus, the effect of the presence of PC in THF solutions as shown in Figure 1 is well explained.

## Conclusion

THF solutions are very good model electrolyte systems for the study of failure and stabilization mechanisms of Li−graphite intercalation anodes because several types of behavior of these electrodes are observed in THF solutions, depending on the presence of additives.

In dry THF or PC solutions, lithium does not intercalate into graphite reversibly. The reason for this is the detrimental surface reactions that occur in the potential window 1−0.3 V ($Li/Li^+$) in which solvent molecules are reduced to organic Li salts (ROLi and $ROCO_2Li$ for THF and PC, respectively). Results obtained from chronopotentiometry, chronoamperometry, XRD impedance spectroscopy, and electron microscopy lead to the conclusion that these solvent reduction products do not passivate the electrode properly (in the specific case of graphite electrodes), and thus a large amount of solvent molecules are reduced until the process is stopped due to the precipitation of thick and resistive surface films. The charge involved in this process is close to the full capacity of the electrode (1 molar equiv per $C_6$). These processes are also accompanied by an increase in the electrodes' surface area due to some exfoliation in the graphite particles. We assume that these initial exfoliation processes on the graphite surface initiate cracking and splitting of graphite particles. These macroscopic processes change the structure of the electrode and its particle orientation. They enable electrical isolation of graphite particles by surface species formed by the reduction of solvent molecules that diffuse into the cracks, between particles, and between particles and the current collector.

It should be mentioned that $LiAsF_6$ reduction also takes place on the graphite surface at potentials between 1.5 and 1 V ($Li/Li^+$), but it does not play an important role in the stabilization or destabilization of these electrodes. When the THF solutions are wet (40 ppm $H_2O$ and above), or when the solutions contain a small concentration of PC (1 M is an optimum), the surface chemistry changes considerably; the surface species precipitated form passivating surface layers that behave like a protective envelope, which prevents massive reduction of solution species. The charge involved in their formation until the electrodes are fully passivated is only about one-third of a full electrode capacity.

In the case of water contamination, it is probable that Li oxide is precipitated as a thin film and thus suppresses THF reduction. At low PC concentration, the surface films formed on graphite contain $Li_2CO_3$, which is an excellent passivating agent. A mechanism for $Li_2CO_3$ precipitation may involve the formation of an unpaired nucleophilic carbonate anion ($CO_3^{2-}$ or $LiCO_3^-$), which at high PC concentration nucleophilically attacks another PC molecule to form the usually observed $ROCO_2Li$ surface species. At low PC concentration, these anions interact preferentially with $Li^+$ and thus precipitate as unreactive, solid $Li_2CO_3$.

**Acknowledgment.** This research was partially financed by the Israeli Ministry of Science and Technology.

## References and Notes

(1) Matsumura, Y.; Wang, S.; Mondori, J. *J. Electrochem. Soc.* **1995**, *142*, 2914.

(2) Aurbach, D.; Chusid, Youngman O.; Carmeli, Y.; Babai, M.; Ein-Eli, Y. *J. Power Sources* **1993**, *43*, 47.

(3) Peled, E. In *Rechargeable lithium and lithium ion batteries*; Megahed, S.; Barnett, B. M.; Xie, L., Eds.; The Electrochemical Society Softbound Series PV 94-28, The Electrochemical Society Inc.: Pennington, NJ, 1995; pp 1−15.

(4) Peled, R. In *Li batteries*; Gabano, J. P., Ed.; Academic Press: New York, London, 1983; Chapter 3.

(5) Aurbach, D.; Ein-Eli, Y. Chusid, O.; Babai, M.; Carmeli, Y.; Yamin, H. *J. Electrochem. Soc.* **1994**, *141*, 603.

(6) Aurbach, D.; Ein-Eli, Y.; Markovsky, B.; Carmeli, Y.; Yamin, H.; Luski, S. *Electrochim. Acta* **1994**, *39*, 2559.

(7) Zhang, Z. In *Rechargeable lithium and lithium ion batteries*; Megahed, S., Barnett, B. M., Xie, L. Eds.; The Electrochemical Society Inc.: Penning, NJ, **1995**; pp 165−182.

(8) Fauteux, D.; Koksbang, R. *J. Appl. Electrochem*. **1933**, *23*, 1, and references therein.

(9) Dahn, J. R.; Sleigh, A. K.; Shi, H.; Way, B. M.; Weydanz, W. J.; Reimers, J. N.; Zhong, Q.; von Sacken, U. In *Lithium batteries, new materials, developments and perspectives*; Pistoia, G., Ed.; Elsevier: Amsterdam, London, New York, Tokyo, 1994; Chapter 1, pp 1−47, and references therein.

(10) Yazami, R. *Ibid*., Chapter 2, pp 49−91, and references therein.

(11) Tatsumi, K.; Iwashita, N.; Sakaebe, H.; Shioyama, H.; Higuchi, S.; Mabuchi, A.; Fujimoto, H.; *J. Electrochem. Soc.* **1995**, *142*, 716.

(12) Sleigh, A. K.; von Sacken, U. *Solid State Ionics* **1992**, *57*, 99.

(13) Zheng, T.; Liu, Y.; Fuller, E. W.; Tseng, S.; von Sacken, U.; Dahn, J. R. *J. Electrochem. Soc.* **1995**, *142*, 2581.

(14) Almagir, M.; Zao, Q.; Abraham, K. M. *J. Electrochem. Soc.* **1994**, *141*, L143.

(15) Dominey, L. A. In *Lithium batteries, new materials, developments and perspectives*; Pistoia, G., Ed.; Elsevier: Amsterdam, London, New York, Tokyo, 1994; Chapter 4, pp 167−238, and references therein.

(16) Fong, R.; von Sacken, U.; Dahn, J. R. *J. Electrochem. Soc.* **1990**, *137*, 2009.

(17) Aurbach, D.; Ein-Eli, Y.; Markovsky, B.; Zaban, A. *J. Electrochem. Soc.* **1995**, *142*, 2882.

(18) Besenhard, J. O.; Winter, M.; Yang, J.; Biberacher, W. *J. Power Sources* **1995**, *54*, 228.

(19) Aurbach, D.; Ein-Eli, Y. *J. Electrochem. Soc.* **1995**, *142*, 1746.

(20) Takai, K.; Tereda, N.; Kumai, K.; Iwahori, T.; Uwai, T.; Miura, T. *J. Power Sources* **1995**, *55*, 191. Moshtev, R. V.; Zlatilova, P.; Puresheva, B.; Manev, V. *Ibid*. **1995**, *56*, 137.

(21) Huang, C. K.; Ratnakumar, B. V.; Surampudi, S.; Halpert, G. In *Rechargeable lithium and Li ion batteries*; Megahed, S., Barnett, B. M., Xie, L., Eds.; The Electrochemical Society Softbound Series PV 94-28; The Electrochemical Society: Pennington, NJ, 1995; pp 361−369.

(22) Aurbach, D.; Markovsky, B.; Schechter, A.; Ein-Eli, Y.; Cohen.; H. *J. Electrochem. Soc*. **1996**, *143*, 3809.

(23) Yamamoto, O.; Imanishi, N.; Takeda, Y.; Kashiwagi, H. *J. Power Sources* **1995**, *54*, 72.

(24) Shu, Z. X.; McMillan, R. S.; Murray, J. J.; Davidson, I. J. *J. Electrochem. Soc*., **1995**, *142*, L161.

(25) Jiang, Z.; Alamgir, M.; Abraham, K. M. *J. Electrochem. Soc*. **1995**, *142*, 333.

(26) Nanjundiah, C.; Goldman, J. L.; Dominey, L. A.; Kock, V. R. *J. Electrochem. Soc*. **1988**, *135*.

(27) Aurbach, D.; Zaban, A. *J. Electroanalytical Chem*. **1995**, *393*, 43.

(28) Billard, D.; Henry, F.; Willman, P. *Mol. Cryst. Liq. Cryst*. **1994**, *245*, 159.

(29) Aurbach, D.; Levi, M. D. *J. Phys. Chem*., submitted.

(30) Aurbach, D.; Zaban, A. *J. Electrochem. Soc*. **1994**, *141*, 1808.

(31) Aurbach, D.; Chusid, O. *J. Electrochem. Soc*. **1993**, *140*, L155.

(32) Aurbach, D.; Daroux, M. L.; Faguy, P.; Yeager, E. *J. Electroanal. Chem*. **1991**, *297*, 225.

(33) Aurbach, D.; Gofer, Y.; Ben-Zion, M.; Aped, P. *J. Electroanal. Chem*. **1992**, *339*, 451.